Electro-optical properties of solution processed OLEDs with phosphorescent heteroleptic Ir(III) complexes: combined effect of different electron withdrawing and bulky substituents bound to the cyclometalating ligands

Wojciech Mróz [a], Roberta Ragni [b], Francesco Galeotti [a], Chiara Botta [a], Ernesto Mesto[b], Luisa De Cola[c], Gianluca Maria Farinola [b] and Umberto Giovanella [a]*

[a] *ISMAC-CNR, Via Bassini 15, 20133 Milano, Italy*
[b] *Dipartimento di Chimica, Università degli Studi di Bari "Aldo Moro", Via Orabona 4, 70126 Bari, Italy*
[c] *Institut de Science et d'Ingénierie Supramoléculaires ISIS, Université de Strasbourg, 8 allée Gaspard Monge 67083 Strasbourg Cedex, France*

Abstract

Orange and green phosphorescent heteroleptic iridium complexes **1** and **2** [**1**: iridium(III)bis[2-(5'-benzylsulfonyl)phenylpyridinato-N,C2']-(2,4-decanedionate), **2**: iridium(III)bis[2-(5'-benzylsulfonyl-3',6'-difluoro)phenylpyridinato-N,C2']-(2,4-decanedionate)], bearing one 2,4-decandionate and two phenylpyridine (ppy) ligands functionalized with electron withdrawing benzylsulfonyl and fluorine substituents, are used as dopant emitters in solution processed organic light-emitting diodes. The effect of these substituents on the phenylpyridine ligands as well as of the long alkyl chain on the 2,4-decandionate ligand was investigated by comparing the photophysical properties and performance in devices of **1** and **2** to those recorded for the green emitting reference phosphor **Ir(ppy)$_2$(acac)** [iridium(III)bis(2-phenylpyridinato-N,C2')-acetylacetonate]. In particular, functionalization of the phenylpyridine ligands with the benzylsulfonyl group enhances the photoluminescence quantum yield (Φ) and red shifts the emission of complex **1** with respect to Ir(ppy$_2$)acac. Further functionalization of the same ligand with two fluorine atoms in **2** restores the green emission observed for the reference complex, yielding even higher Φ. Hence, combination of the two kinds of substituents represents a suitable functionalization pattern to increase the photoluminescence efficiency of **2** *vs* the unfunctionalized Ir(ppy)$_2$(acac). Moreover, the bulky effect of both benzylsulfonyl groups in 2-phenylpyridines and of the alkyl chain in the β-diketonate ligand, as well as the enhanced electron

mobility induced by fluorine atoms, are supposed to be responsible for high external quantum efficiency (EQE up to 12 %) and high luminous efficiency (η_L up to 24.2 cd/A) for a **2** based fully solution processed PHOLED with properly tailored architecture which includes an electron transporting layer of a PEG substituted polyfluorene (PEG: poly(ethylene glycol)). This device outperforms the control diode based on $Ir(ppy)_2(acac)$ (EQE 5.5% and η_L 17 cd/A) and approaches the best efficiencies achieved thus far for green Ir(III) complex based PHOLEDs made by vacuum thermal deposition technique.

Introduction

According to scientific and industrial research in the last decade, cyclometalated iridium(III) complexes have come out on top of suitable phosphorescent emitters for optoelectronic, sensing and biomedical applications [1]. High photoluminescence quantum yield (Φ) and good solubility of these emitters in organic solvents have allowed the fabrication of phosphorescent light-emitting devices (PHOLEDs) with up to 100% internal quantum efficiency by wet processes involving the deposition of the emitting layer from a solution of iridium phosphor, used as the dopant, and an organic polymeric or molecular material used as the host matrix [2]. Heteroleptic $Ir(C^N)_2LX$ complexes (C^N=2-arylpyridinato, LX= third different ancillary ligand) have found extensive application in PHOLEDs because of their more sustainable production and easier synthetic accessibility with respect to the homoleptic $Ir(C^N)_3$ counterparts whose synthetic procedures require fine control of reaction temperatures [3].

An appealing feature of this class of emitters lies in their excellent emission colour tunability by proper chemical design of organic ligands bound to iridium ion. Emission properties of heteroleptic iridium complexes are mainly governed by the chemical structure of the C^N ligand, with a secondary role also played by the nature of the ancillary LX ligand [4]. Moreover, electronic effects and position of substituents bound to the C^N ligand play a key role in determining the emission colour of heteroleptic complexes [5], influencing their highest occupied (HOMO) and lowest unoccupied molecular orbital (LUMO) energy levels, alike sterical hindrance and charge transport ability of substituents can influence quantum efficiencies of the corresponding devices made with these phosphors [6].

Indeed, C^N ligands with planar non hindered structure generally enable relatively strong intermolecular π–π interactions leading to the formation of small Ir(III) complexes crystallites responsible for detrimental self-quenching [7] by triplet–triplet annihilation (TTA) and hence to the

decrease of device electroluminescence (EL) efficiency. A suitable approach to reduce the aggregation tendency of iridium complexes, mainly under prolonged electric stress, and to enhance their solution-processability and stability in amorphous phase consists in the introduction of bulky substituents, such as dendritic, bicyclic or spiro groups, that break the molecular planarity of cyclometalated organic ligands. As a consequence, a reduction of the intermolecular π–π interactions responsible for aggregate formation of iridium complexes in the solid state is observed, thus enhancing their quantum efficiency in devices [8].

On this ground, we synthesized a series of heteroleptic iridium complexes bearing one 2,4-decandionate and two 2-phenylpyridine ligands functionalized, in various alternative positions, with sterically hindered electron withdrawing benzylsulfonyl groups: in particular, we observed a strong dependence of the HOMO-LUMO energy gap and emission colour of these phosphors on the position of such substituents in the ligands [9]. Moreover, the combined effect of benzylsulfonyl groups and fluorine atoms, on photophysical properties of these iridium complexes in solution was studied. Indeed, fluorination is a well-known suitable approach to tune (blue-shift) the emission colour, to enhance electron mobility and to prevent close packing that favours self-quenching of the emission in materials for optoelectronic applications [10]. Moreover, the 2,4-decandionate used as the third ancillary ligand in place of the most common acetylacetonate was selected to improve the solubility of complexes in organic solvents. As a further effect, the long alkyl chain in 2,4-decandionate was expected to contribute to sterical hindrance and, therefore, to reduce triplet-triplet annihilation of these complexes in the solid state, thus enhancing their electroluminescence efficiency in devices.

Here we report the application of these emitters in PHOLEDs: in particular, to investigate the effects of benzylsulfonyl, fluorine and alkyl substituents on devices efficiency, we compared performances of PHOLEDs made with the complexes **1** and **2** (Figure 1), with those ones observed for their analogue made with the unsubstituted **Ir(ppy)$_2$(acac)** used as the reference phosphor.

Moreover, we demonstrate the possibility to optimize device performances by properly selecting the multilayer architecture and, in particular, by using an electron injecting/transporting layer (ETL) based on a polyfluorene bearing poly(ethylene glycol) (PEG) side groups.

Bilayer devices fabricated by fully solution deposition of the emitting and the electron transporting layers show performances approaching the best ones reported in the literature for diodes prepared by vacuum deposition technique with Ir(III) complexes emitting in similar spectral range [11].

Results and discussion

Substitution effects on photophysical properties of iridium complexes

The heteroleptic complexes **1** and **2** shown in Figure 1 were prepared according to the literature by a double-step synthetic procedure involving the preliminary synthesis of dichloro bridged dimer iridium complexes from the corresponding functionalized 2-phenylpyridine ligands and iridium chloride trihydrate, and their subsequent reaction with the 2,4-decandione in the presence of sodium carbonate as the base [9].

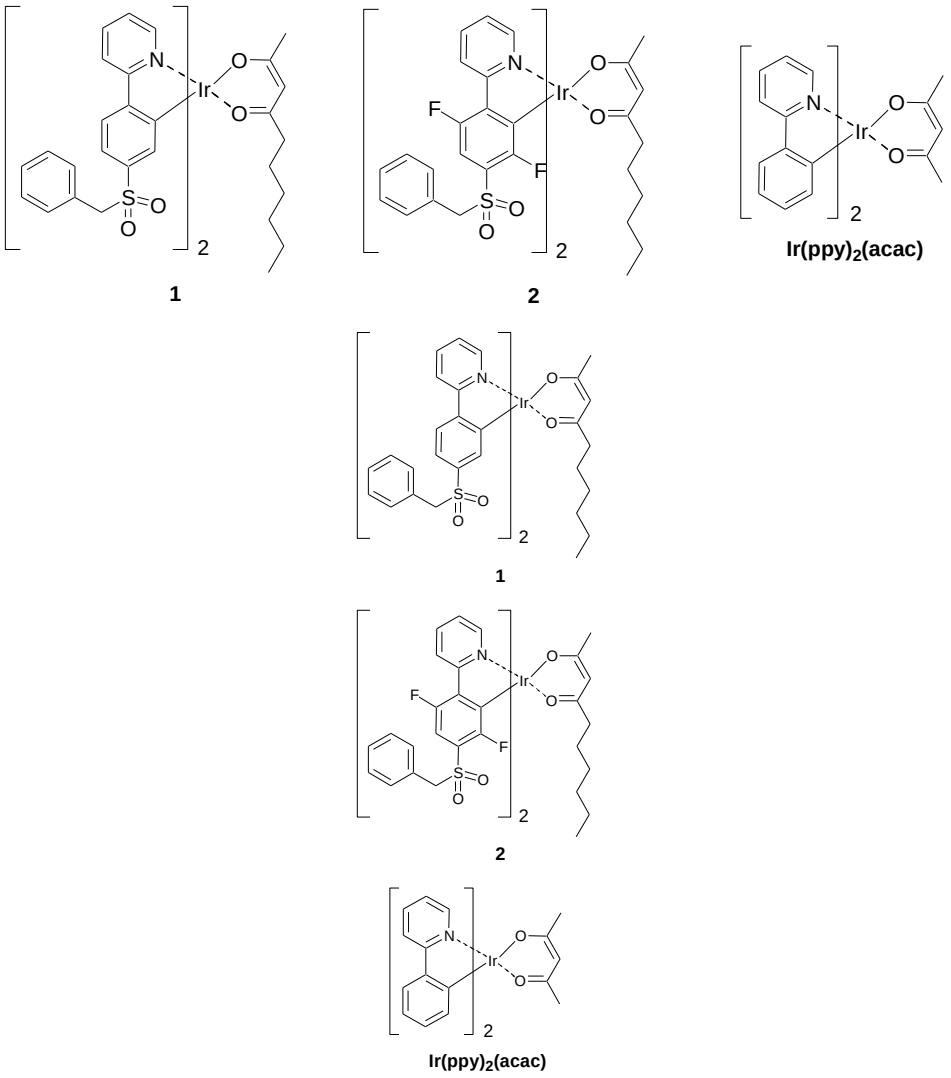

Figure 1. Chemical structures of complexes **1**, **2** and **Ir(ppy)$_2$(acac)**

Photophysical and electrochemical properties of **1** and **2** were investigated in our previous work and are here summarized in Table 1 to compare them to those reported in the literature for the unsubstituted reference complex **Ir(ppy)$_2$(acac)** [9,12,13].

Table 1. Summary of photophysical and electrochemical properties of complexes **1**, **2** and **Ir(ppy)$_2$(acac)**.

Complex	λ_{PL} (nm)	τ (μs) 298K	τ (μs) 77K	Φ	$E_{1/2}$ (Red) [V]	$E_{1/2}$ (Ox) [V]	E^{HOMO} (eV)	E^{LUMO} (eV)
1	546[a]	2.7[a]	7.6[b]	0.71[d]	-1.33	0.67	-5.47	-2.65
2	515[a]	3.0[a]	6.9[b]	0.65[d]	-1.42	0.98	-5.77	-2.8
Ir(ppy)$_2$(acac) [12,13]	516[c]	1.6[c]	3.2[a]	0.34[c]			-5.20	-2.19

[a] in degassed dichloromethane, [b] in butyronitrile, [c] in 2-MeTHF, [d] in degassed dichloromethane *vs.*quinine disulfate in 0.5 M H_2SO_4 (λ_{exc}=343 nm). HOMO and LUMO energies have been calculated from $E_{1/2}$ redox potentials measured by cyclic voltammetry as reported in the literature [ref1].

In the case of heteroleptic Ir(ppy)$_2$(LX) complexes that contain 2-phenylpyridine ligands, , it is well known that the HOMO mainly comprises the iridium d orbitals and the phenyl π orbitals on the 2-phenylpyridines, whereas the LUMO is mainly comprised of the π* orbitals on the pyridyl rings [ref2]. Hence, the introduction of electron-withdrawing substituents, such as fluorine atoms, to the phenyl rings of ppy ligands usually decreases the HOMO energy while keeping the LUMO level relatively unchanged. This effect leads to an increase of the HOMO-LUMO energy gap and to a blue shift of the emission. [ref3]

Contrary to this common trend, functionalization with the electron withdrawing benzylsulfonyl group of the C^N ligand phenyl ring in the *meta* position to iridium decreases both the HOMO and LUMO levels (Table 1) with more pronounced effect on the LUMO, thus leading to a reduction of the HOMO-LUMO gap and to a 30 nm red-shift of emission of the orange phosphor **1** with respect to the green emitting unsubstituted **Ir(ppy)$_2$(acac)** (λ_{PL} = 546 nm *vs* 516 nm). This effect could be explained considering that the sterically hindered benzylsulfonyl group of one phenylpyridine (ppy) ligand in complex **1** may be spatially located nearby the pyridine ring of the other ppy ligand. We observed this

spatial proximity in the crystal structure of an iridium dimer complex (**3** in Figure **2**) bearing, around each iridium ion, two ppy ligands in the same arrangement and with the same benzylsulfonyl functionalization observed in complex **2** [ref4] .

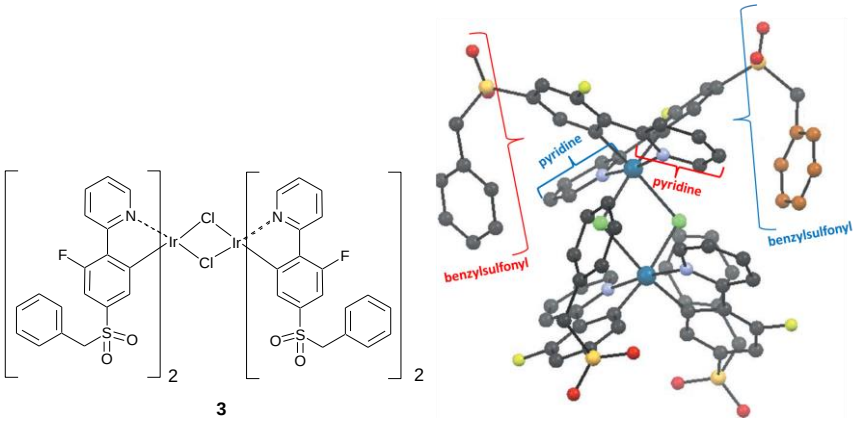

3

Figure 2 Chemical and X.ray structure of complex **3** functionalized with benzylsulfonyl groups in *meta* position to iridium. The pyridine rings and benzylsulfonyl groups belonging to the same 2-phenylpyridine ligand bound to one iridium ion are highlighted by parenthesis (in blue and red colour for each ligand). The benzylsulfonyl group in red (or blue) colour is close to the pyridine ring in blue (or red) colour. Figure adapted with permission from ref.3. Copyright 2013. WILEY-VCH Verlag GmbH & Co. KGaA, Weinheim

This spatial disposition may cause an interaction between the electron withdrawing benzylsulfonyl groups and the electronic density of the neighbouring pyridine rings, with more pronounced reduction of the LUMO energy causing the red-shift of the emission. Moreover, a significant increase of the photoluminescence quantum yield was observed for complex **1** (Φ = 0.71 *vs* 0.34 of $Ir(ppy)_2acac$), likely due to the sterical hindrance of both the benzylsulfonyl substituents in phenylpyridines and the alkyl group in decandionate around iridium ion that may prevent the emission quenching.

Further functionalization of phenylpyridines with two electron withdrawing fluorine atoms in *meta* and, more importantly, in *orto* position to iridium lowers the energy of the HOMO level, and hence enhances the HOMO-LUMO gap, inducing a 30 nm blue-shift of complex **2** emission versus complex **1**. As a consequence, the bathochromic shift imposed by having the benzylsulfonyl group *meta* to the iridium is balanced by the hypsochromic shift due to the electron-withdrawing fluorine atoms. This contribution leads to a green emission for **2** (λ_{PL} = 515 nm), similar to the emission of **$Ir(ppy)_2(acac)$** (λ_{PL} = 516 nm), whereas a higher value of the photoluminescence quantum yield (0.65) is maintained for the functionalized emitter versus the reference complex [12].

Electroluminescence

The most effective approach to fabricate efficient solution processed PHOLEDs is to deposit the emitting layer (EML) by spin-coating the phosphorescent dopants **1** or **2**, mixed with a suitable host material, such as the polyvinylcarbazole (PVK in Figure 1). PVK, due to its high E_T level located at 2.5 eV [13], is able to confine excitons at the complex molecules, because triplet levels of **1** and **2** are located at lower energies than in PVK, preventing energy back transfer to the matrix. Moreover, the addition of 1,3-bis(5-(4-tert-butylphenyl)-1,3,4-oxadiazol-2-yl)benzene (OXD7) to the blend of the iridium phosphor and PVK improves charge carrier balance within the EML. Therefore, as reported in Figure 1a, PHOLEDs were firstly fabricated with the basic structure ITO / PEDOT:PSS / 65% PVK : 30% OXD7 : 5% Ir(III) complex /Ba/Al (device A) by spin-coating the blend of the green (**1**) or orange (**2**) phosphor dopant, the electron transporting OXD7 and the PVK host material (Figure 3). The reference device with **Ir(ppy)$_2$(acac)** was built in the same way.

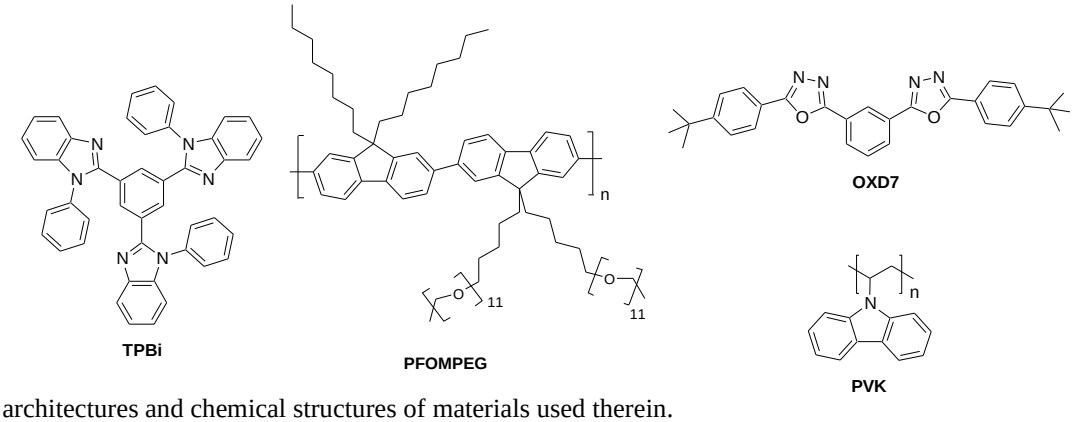

Figure 3. Device architectures and chemical structures of materials used therein.

Electroluminescence spectra and related CIE coordinates of these devices are shown in Figure 4a. EL peaks are at 546 nm for **1**, 512 nm for **2** and at 523nm for **Ir(ppy)$_2$(acac)**, respectively. Poorly resolved vibrational structures of the spectra suggest the dominant role of ^{3}MLCT states in the electroluminescence emission [4b,14]. The CIE coordinates (0.31, 0.64) are recorded for the **Ir(ppy)$_2$(acac)** based device, (0.45, 0.54) for the PHOLED made with the benzylsulfonyl functionalized complex **1** and (0.31, 0.62) for the fluorine substituted complex **2** based diode.

Representative current density-voltage-luminance (J-V-L) curves and EQE plots of the basic devices are presented in Figure 4b. The turn on voltage (V_{on}) of devices with **1** and **2** is 8 V although PHOLED with complex **2** revealed more rapid current and luminance increase than PHOLED with complex **1**. Reference diode showed lower V_{on} most likely due to smaller thickness of the EML (see table 2).

a)

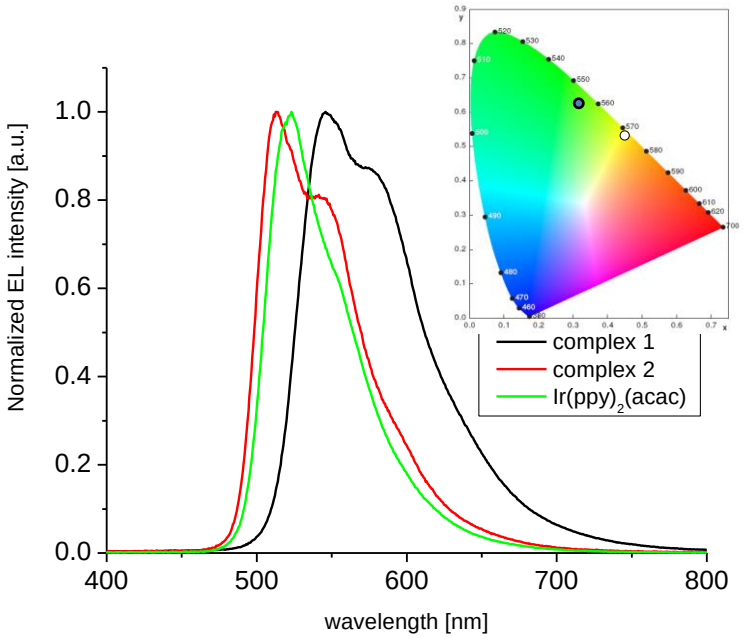

b)

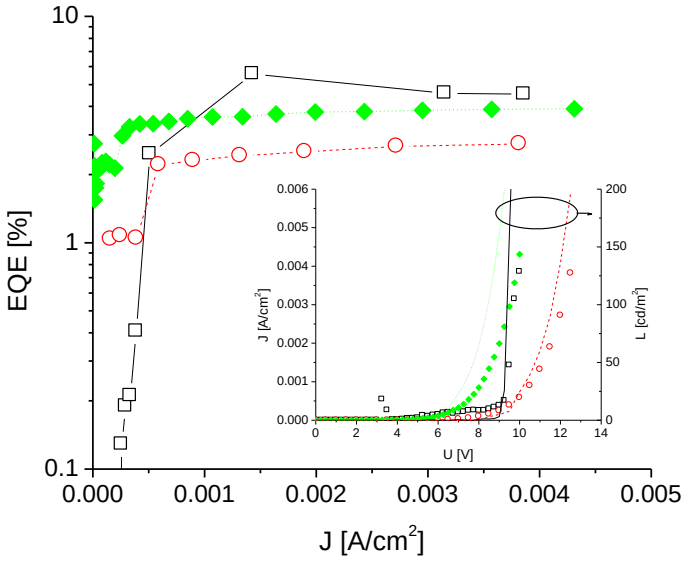

Figure 4. a) EL spectra of PHOLEDs with emissive layer 65% PVK : 30% OXD7 : 5% Ir complex: complex **1** (black), complex **2** (red), **Ir(ppy)$_2$(acac)** (green); in the inset, CIE coordinates corresponding to the EL spectra of PHOLEDs based on complex **1** (empty circle) and complex **2** (black circle). b) EQE versus J of devices with structure PEDOT:PSS / 65% PVK : 30% OXD7 : 5% Ir complex / Ba / Al; black squares and solid line for **2** as a dopant; red circles and dashed line for **1** as a dopant; and green diamonds and dotted line for **Ir(ppy)$_2$(acac)** as dopant. Inset, representative J–V–L curves of the devices.

Maximum values of EQE and LE of PHOLED based on complex **2** (EQE = 5.56 %, LE =11.4 cd/A) are about two times better than those recorded for complex **1** (EQE = 2.86 %, LE = 5.4 cd/A) despite their similar values of quantum yields in de-aerated dichloromethane solution (0.71 and 0.65 for **1** and **2**, respectively). Maximal EQE and LE of control device are 4.09 % and 8.5 cd/A, with intermediate values of efficiency with respect to complex **1** and **2**. We tentatively ascribe the different behaviour observed in **1** and **2** based PHOLEDs to different localizations of the recombination zones in EML, dependending on energy levels of complexes and also on their charge transporting properties. In case of the device made with complex **1**, electrons could travel with some difficulty toward the centre of the emissive layer due to the mismatch of LUMO levels of **1** and of OXD7 while holes can move easily through the EML (see figure 5). Therefore, recombination zone can be expected at the proximity of the cathode. Considering the diode made with complex **2**, electrons do not encounter energy barriers due to the alignment of LUMO levels of **2** and OXD7, as well as possible favourable influence of the electron transporting properties induced by fluorine substituents [15]. On the other hand, hole transport is slowed down by deep HOMO energy level of the complex **2**. Recombination zone of the device made with **2** is expected to be localized closer to PEDOT:PSS / EML interface. Similarly, recombination zone closer to PEDOT:PSS is expected in PHOLED with **Ir(ppy)$_2$(acac)**, due to hole trapping at the Ir(III) complex.

It is well known that a significant part of OLEDs emission is lost due to the generation of plasmons in a cathode [16] and exciton quenching on defects at the EML/cathode interface [17]. By moving the recombination zone farther from the electrode this loss can be reduced and so efficiency of a device increased, as evident in this case.

Values of critical current density $J_{90\%}$, defined as current density J at which the EQE decreases to 90% of the maximal value, are reported for all diodes in Table 2. High critical current densities are crucial to obtain efficient devices with long lifetimes, because the lifetime of an OLED decreases in proportion to J^{-n} (n = 1.2–1.9, called the acceleration factor) [18]. Therefore, if a device is able to sustain high performance at high current density, it is expected to last longer than the one with lower $J_{90\%}$, both at a chosen luminance level. Critical current density values of OLEDs based on **1** and **2** (8-40 mA/cm^2) are within the range of $J_{90\%}$ reported for other materials [19], making them good emitter candidates for OLEDs.

Device optimization

To optimize performances of devices and to investigate potentiality of the functionalized phosphors here discussed, the improvement of both charge carrier injection and their confinement within the EML has been accomplished by inserting a polymeric ETL on top of the EML (device B, Figure 1b). It is known that poly(ethylene glycol) (PEG)-bearing materials promote electron injection from metal and are therefore effective in the confinement of the emissive region far from the electrode [20]. In order to have a fully solution processable device we have used a PEG functionalized fluorene derivative (PFOMPEG in Figure 3) [21] deposited directly on the emitting layer from alcohol solution (Figure 3b). Alternatively, a 2,2',2"-(1,3,5-benzinetriyl)-tris(1-phenyl-1-H-benzimidazole) (TPBi) layer was thermally sublimed in high vacuum (device C, Figure 3c) as ETL with similar features as PFOMPEG.

The multilayer structure of devices slightly affects the EL spectrum profile, likely because of different thicknesses of OLEDs that change cavity resonance conditions (spectra of all types of diodes are gathered in Supporting Information, fig. S1).

On the other hand, a huge difference in devices performance is observed. LE of optimized devices B and C are presented in Figure 5. OLEDs based on **1** (device C) and **2** (device B) doubled the EQEs and LEs of corresponding devices A without the optimized ETL. Diode containing complex **1** improved EQE from 2.86 % to 5.3 % by inserting the TPBi layer, preferred instead of PFOMPEG, since higher efficiencies were recorded. More interestingly, the PFOMPEG interlayer in diode doped with complex **2** enhanced EQE from 5.56 % to 11.98 % and LE from 11.4 cd/A to 24.2 cd/A, and increased almost three fold PE with respect to device A. Differently, the use of ETL had less impact on efficiency of the reference diode. All results of the basic and optimized devices are summarized in Table 2.

Table 2. Performance of diodes under investigation

	V_{on} [V]	$J_{90\%}$[a] [A/cm^2]	thickness [nm]	EQE_{max}[b] [%]	LE_{max}[c] [cd/A]	PE_{max}[c] [lm/W]	L_{max}[c] [cd/m^2]	CIE (x, y)
PVK:OXD7: **1**	8	0.040	162	2.86	5.4	1.31	3668	0.448, 0.539
PVK:OXD7: **2**	8	0.008	140	5.56	11.4	3.76	3350	0.316, 0.619
PVK:OXD7: **Ir(ppy)$_2$(acac)**	5	0.08	128	4.09	8.5	3.70	13646	0.307, 0.639
PVK:OXD7: **1** / TPBi	6	0.023	188	5.30	10.5	3.86	4288	0.411, 0.562
PVK:OXD7: **2** / PFOMPEG	6	0.022	147	11.98	24.2	11.07	7100	0.330, 0.607
PVK:OXD7: **Ir(ppy)$_2$(acac)** / PFOMPEG	4	0.006	136	5.53	11.7	5.76	2743	0.303, 0.635

[a] critical current density defined as current density at which the EQE drops to 90% of its maximum value, [b] total maximal external quantum efficiency, [c] maximal value in forward direction

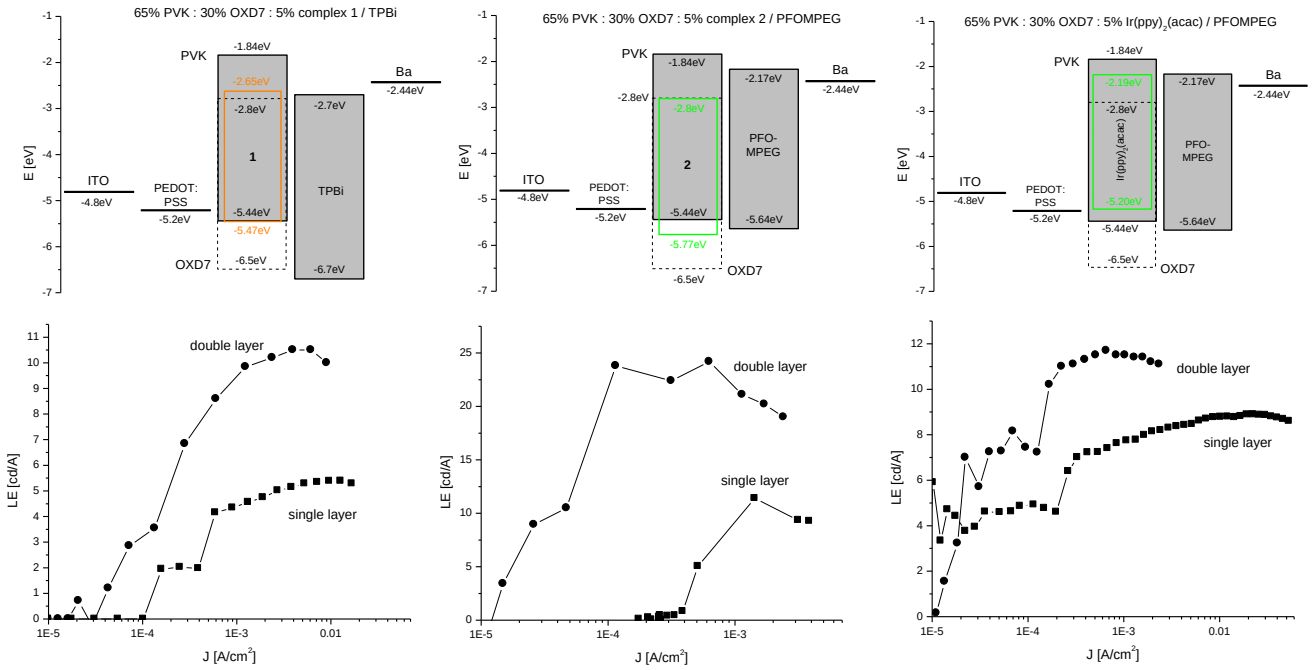

Figure 5. Energy levels of materials used in OLEDs with complex **1** (top left), **2** (top middle) and **Ir(ppy)$_2$(acac)** (top right) as dopants. For details of specific diode composition see in text. Luminous efficacies of devices with complex **1** (bottom left), complex **2** (bottom middle) and **Ir(ppy)$_2$(acac)** (bottom right) as emitters

A better charge balance and localization of recombination zone within the EML in the device B based on complex **2**, due to the appropriate LUMO alignment between materials in the EML and likely due to improved electron transporting properties granted by fluorine atoms, can be identified as the main reason for the EQE two fold increase in comparison to the device C made with **1**.

Energy transfer mechanism from the matrix to the complexes can be reasonably neglected in an attempt to explain differences in EQE of the three diodes due to similarly small values of extinction coefficients of the complexes [9,12] in the spectral range of PVK and OXD7 emission. For the same reason exciton exchange between triplet state of PVK and complex **2**, as for the triplet state of TPD and Ir(ppy)$_3$, [22] is not efficient and cannot explain higher efficiency of the fluorinated complex in comparison to the non fluorinated counterpart.

The insertion of ETL layers, both TPBi and PFOMPEG, resulted in decrease of V_{on} (figure S2). If we consider the energy levels of TPBi, V_{on} reduction can be primarily attributed to hole blocking properties of TPBi. Highly concentrated holes attract electrons, thus creating depletion zone in ETL and facilitating injection of electrons from the cathode. In the case of PFOMPEG, the reduction of V_{on} can be ascribed to a promoted electron injection from metals [20].

Conclusions

In conclusion, we have investigated the electronic and sterical effects of the benzylsulfonyl, fluorine and alkyl substituents on performances and emission colour of the heteroleptic complexes **1** and **2** in solution processed PHOLEDs. These effects have been evaluated by comparison of devices incorporating **1** and **2** as the emissive materials with a reference **Ir(ppy)$_2$(acac)** based diode.

In particular, we have explained the reason why the bulky electron withdrawing benzylsulfonyl groups bound to ppy phenyl rings of complex **1** in *meta* position to iridium induce a red-shift of photo- and electroluminescence, as well as higher EQE, of **1** based devices *vs* the reference complex. Further functionalization with two electron withdrawing fluorine atoms in complex **2** allows to balance the red shift induced by the benzylsulfonyl groups, still keeping high external quantum and luminous efficiencies, in fully solution processed green emitting device made with complex **2** (EQE 12 % of EQE and 24.2 cd/A) These performances are comapable to the the best efficiencies achieved thus far for green Ir(III) complex based PHOLEDs made by vacuum thermal deposition technique. Therefore, complexes **1** and **2** have been demonstrated to be promising orange and green phosphors suitable for organic display technology based on solution processing of the emitting layer.

Experimental

Materials

The heteroleptic complexes **1** and **2** were prepared according to the literature [9]. PVK, OXD7 and TPBi were used as purchased while PFOMPEG was synthesized according to the reference [21].

Devices

Indium tin oxide substrates (ITO, 15 Ω/sqr) were cleaned ultrasonically in distilled water, acetone and 2-propanol. On substrates water solution of poly-(3,4-ethylenedioxythiophene)-poly-(styrenesulfonic acid) (PEDOT:PSS, Clevios P VP AI 4083, H. C. Starck) was spin coated through nylon filter (pore size 0.45μm), creating 50 nm thick hole injecting layers. Subsequently substrates were annealed for 10 minutes at 100^{o}C inside nitrogen filled glovebox. In single and double layer devices, emissive layers were deposited on ITO substrates covered with PEDOT:PSS. Emissive layers (EML) consisted of 65% PVK : 30% OXD7 : 5% Ir complex (w/w), where poly-(N-vinylcarbazole) PVK has M_w=(25-50)·10^{3}g/mol (Sigma-Aldrich). Solutions containing mixture of PVK, OXD7 and the complexes were spin coated from deaerated chlorobenzene with concentration 15mg/ml. In case of double layer

devices, on emissive layer containing **1**, 2,2',2''-(1,3,5-benzinetriyl)-tris(1-phenyl-1-H-benzimidazole) (TPBi, Ontario Chemicals) was deposited from Knudsen cell, while on the EML based on complex **2** electron transporting polymer poly[(9,9-bis(6'-polyethylene oxide hexyl)-fluorene-2,7-diyl)-*alt*-(9,9-di-*n*-octylfuorene-2,7-diyl)] (PFOMPEG) was spin coated from ethanol solution, in both cases creating electron transporting layers (ETL). Preparation of devices was concluded with vacuum evaporation of 7 nm of barium and 80 nm of aluminium at 10^{-6} mbar pressure.

Measurements

Electroluminescence (EL) spectra were measured using CCD combined with monochromator (Spex 270M) and applying constant bias. The current density-voltage-luminance (J-V-L) characteristics were recorded with Keithley 2602 source meter. Light emitted from devices was detected in forward direction using calibrated photodiode. All characterization was performed in nitrogen atmosphere. Thicknesses of devices were measured with Dektak XT (Bruker) profilometer.

Acknowledgements

Authors wish to thank Dr. Barbara Vercelli (CNR-IENI) for electrochemical characterization of PFOMPEG. MIUR-PRIN 2012A4Z2RY_001 ACQUA-SOL is acknowledged for financial support.

Supporting

Fig. S1. Comparison of EL spectra of all devices:

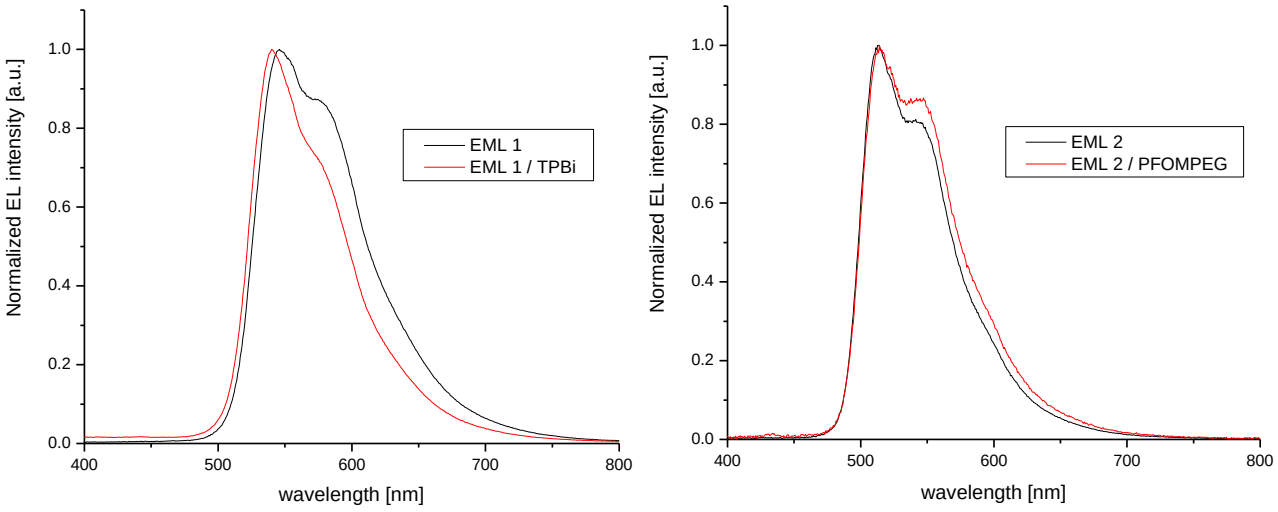

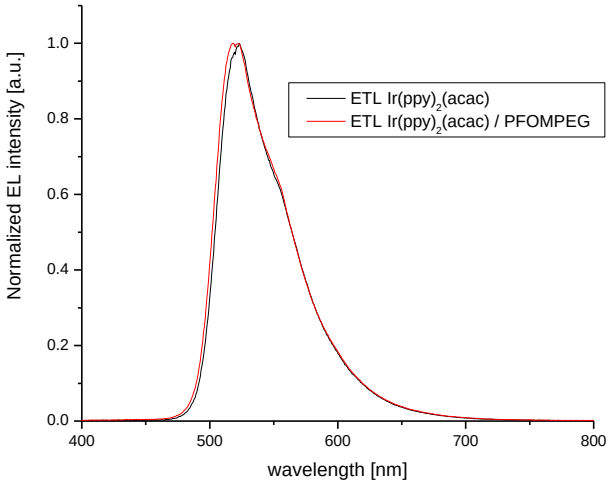

Fig. S2. J-V-L plots of devices with structure 65% PVK : 30% OXD7 : 5% Ir complex (black) and 65% PVK : 30% OXD7 : 5% Ir complex / ETL (red).

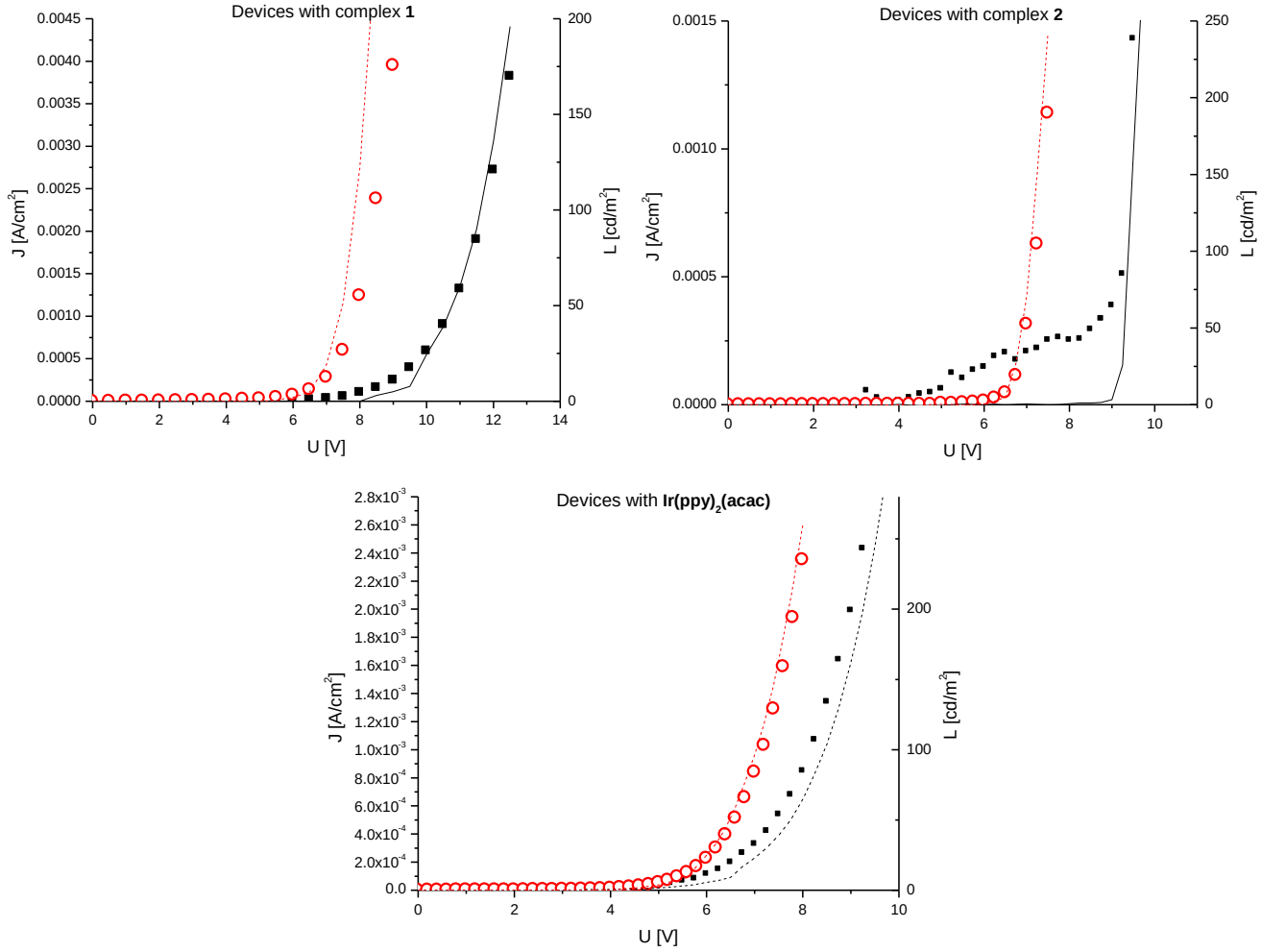

References

[1] (a) C. Ulbricht, B. Beyer, C. Friebe, A. Winter, U. S. Schubert *Adv. Mater.* **2009**, *21*, 4418–4441. (b) G. M. Farinola, R. Ragni *Chem. Soc. Rev.*, 2011, **40**, 3467–3482. (c) G Zhoua, W.-Y. Wongb, S. Suoc *J. Photochem. Photobiol. C: Photochem. Rev.* **2010**, *11*. 133–156]

[2] (a) C. Fan,Y. Li, C. Yang, H. Wu, J. Qin, Y. Cao *Chem. Mater.* **2012**, *24*, 4581−4587. (b) C. Fan, J. Miao, B. Jiang, C. Yang, H. Wu, J. Qin, Y. Cao *Organic Electronics* **2013**, *14*, 3392–3398. (c) J.-H. Jou, S.-H. Peng, C.-I. Chiang, Y.-L. Chen, Y.-X. Lin, Y.-C. Jou, C.-H. Chen, C.-J. Li, W.-B. Wang, S.-M. Shen, S.-Z. Chen, M.-K. Wei, Y.-S. Sun, H.-W. Hung, M.-C. Liu, Y.-P. Lin, J.-Y. Li, C.-W. Wang *J. Mater. Chem. C*, **2013**, *1*, 1680–1686. (d) J.-H. Jou, C.-J. Li, S.-M. Shen, S.-H. Peng, Y.-L. Chen, Y.-C. Jou, J. H. Hong, C.-L. Chin, J.-J. Shyue, S.-P. Chen, J.-Y. Li, P.-H. Wang, C.-C. Chen *J. Mater. Chem. C*, **2013**, *1*, 4201–4208.]

[3] R. Ragni, E. A. Plummer, K. Brunner, J. W. Hofstraat, F. Babudri, G. M. Farinola, F. Naso, L. De Cola *J. Mater. Chem.* **2006**, *16*, 1161–1170]

[4] (a) G. Ge, J. He, H. Guo, F. Wang, D. Zou *J. Organomet. Chem.* **2009**, *694*, 3050–3057. (b) S. Lamansky, P. I. Djurovich, D. Murphy, F. Abdel-Razzaq, H. E. Lee, C. Adachi, P. E. Burrows, S. R. Forrest, M. E. Thompson, *J. Am. Chem. Soc.* **2001**, *123*, 4304-4312]

[5] W.-C. Chang, A. T. Hu, J.-P. Duan, D. K. Rayabarapu, C.-H. Cheng *J. Organomet. Chem.* **2004**, *689*, 4882–4888]

[6] Y. You, S. Y. Park *Dalton Trans.* **2009**, 1267–1282]

[7] S. Takayasu, T. Suzuki, K. Shinozaki *J. Phys. Chem. B* **2013**, *117*, 9449-9456]

[8] (a) S.-C. Lo, N. A. H. Male, J. P. J. Markham, S.W. Magennis, P. L. Burn, O. V. Salata, I. D.W. Samuel, *Adv. Mater.* (Weinheim, Ger.), **2002**, *14*, 975–979. (b) T. D. Anthopoulos, M. J. Frampton, E. B. Namdas, P. L. Burn, I. D. W. Samuel, *Adv. Mater.* (Weinheim, Ger.), **2004**, *16*, 557–560. (c) H. Z. Xie, M. W. Liu, O. Y. Wang, X. H. Zhang, C. S. Lee, L. S. Hung, S. T. Lee,. P. F. Teng, H. L. Kwong, H. Zheng , .C. M. Che *Adv. Mater.* **2001**, *13*, 1245-1248]

[9] R. Ragni, E. Orselli, G. S. Kottas, O. Hassan Omar, F. Babudri, A. Pedone, F. Naso, G. M. Farinola, L. De Cola *Chem. Eur. J.* **2009**, *15*, 136-148]

[10] F. Babudri, G. M. Farinola, F. Naso, R. Ragni *Chem. Commun.* **2007**, 1003-1022]

[11] Jwo-Huei Jou, You-Xing Lin, Shiang-Hou Peng, Chieh-Ju Li, Yu-Min Yang, Chih-Lung Chin, Jing-Jong Shyue, Shih-Sheng Sun, Mandy Lee, Chien-Tien Chen, Ming-Chung Liu, Cheng-Chang Chen, Guan-Yu Chen, Jin-Han Wu, Cheng-Hung Li, Chao-Feng Sung, Mei-Ju Lee, Je-Ping Hu, *Adv Funct Mater* 24 (2014) 555-562; Jwo-Huei Jou, Yu-Min Yang, Sun-Zen Chen, Jing-Ru Tseng,

Shiang-Hau Peng, Chun-Yu Hsieh, You-Xing Lin, Chih-Lung Chin, Jing-Jong Shyue, Shih-Sheng Sun, Chien-Tien Chen, Ching-Wu Wang, Chien-Chih Chen, Shih-Hsiang Lai, Fu-Ching Tung, *Adv Opt Mater* 1 (2013) 657; Guijiang Zhou, Cheuk-Lam Ho, Wai-Yeung Wong, Qi Wang, Dongge Ma, Lixiang Wang, Zhenyang Lin, Todd B. Marder, Andrew Beeby, *Adv Funct Mater* 18 (2008) 499-511]

[12] S. Lamansky, P. Djurovich, D. Murphy, F. Abdel-Razzaq, R. Kwong, I. Tsyba, M. Bortz, B. Mui, R. Bau, M. E. Thompson *Inorg Chem* 40 (2001) 1704-1711]

[13] Fang-Chung Chen, Shun-Chi Chang, Gufeng He, Seungmoon Pyo, Yang Yang, Masayuki Kurotaki, Junji Kido, *Journal of Polymer Science: Part B: Polymer Physics*, 41 (2003) 2681–2690]

[14] A. Tsuboyama, H. Iwawaki, M. Furugori, T. Mukaide, J. Kamatani, S. Igawa, T. Moriyama, S. Miura, T. Takiguchi, S. Okada, M. Hoshino, K. Ueno *J. Am. Chem. Soc.* **2003**, *125*, 12971-12979]

[15] Y. Wang, N. Herron, V. V. Grushin, D. LeCloux, V. Petrov *Appl. Phys. Lett.* **2001**, *79*, 449-451]

[16] (a) A. L. Burin, M. A. Ratner *J. Phys. Chem. A* **2000**, *104*, 4704-4710. (b) S. Nowy, N. A. Reinke, J. Frischeisen, W. Brütting, *Proc. SPIE* **2008**, *6999*, 69992V. (c) S. Nowy, J. Frischeisen, W. Brütting, *Proc. SPIE* **2009**, *7415*, 74151C]

[17] Y. He, S. Gong, R. Hattori, J. Kanicki *Appl. Phys. Lett.* **1999**, *74*, 2265-2267]

[18] T. Tsujimura, "OLED displays: fundamentals and applications", Edit. Anthony C. Lowe, 2012, John Wiley & Sons, Inc., Hoboken, New Jersey, chapter 2]

[19] C. Murawski, K. Leo, M. C. Gather *Adv Mater* 25 (2013) 6801]

[20] R. Trattnig, L. Pevzner, M. Jäger, R. Schlesinger, M. V. Nardi, G. Ligorio, C. Christodoulou, N. Koch, M. Baumgarten, K. Müllen, E. J. W. List, *Adv. Funct. Mater*. 23 (2013) 4897-4905]

[21] J. H. Yao, K. Y. Mya, L. Shen, B. P. He, L. Li, Z. H. Li, Z.-K. Chen, X. Li and K. P. Loh, *Macromol*. 2008, **41**, 1438-1443]

[22] J. Kalinowski, W. Stampor, M. Cocchi, D. Virgili, V. Fattori, P. Di Marco, *Chem Phys* 297 (2004) 39-48]